Meteorol Atmos Phys (2004)
DOI 10.1007/s00703-004-0094-7

Meteorology and Atmospheric Physics
Printed in Austria

[1] Department of Earth System Science, University of California at Irvine, Irvine, CA, USA
[2] NASA/Goddard Space Flight Center, Greenbelt, MD, USA

Contrasting Indian Ocean SST variability with and without ENSO influence: A coupled atmosphere-ocean GCM study

Jin-Yi Yu[1] and **K. M. Lau**[2]

With 10 Figures

Received November 10, 2003; revised April 19, 2004; accepted May 20, 2004
Published online: August 30, 2004

Summary

In this study, we perform experiments with a coupled atmosphere-ocean general circulation model (CGCM) to examine ENSO's influence on the interannual sea-surface temperature (SST) variability of the tropical Indian Ocean. The control experiment includes both the Indian and Pacific Oceans in the ocean model component of the CGCM (the Indo-Pacific Run). The anomaly experiment excludes ENSO's influence by including only the Indian Ocean while prescribing monthly-varying climatological SSTs for the Pacific Ocean (the Indian-Ocean Run). In the Indo-Pacific Run, an oscillatory mode of the Indian Ocean SST variability is identified by a multi-channel singular spectral analysis (MSSA). The oscillatory mode comprises two patterns that can be identified with the Indian Ocean Zonal Mode (IOZM) and a basin-wide warming/cooling mode respectively. In the model, the IOZM peaks about 3–5 months after ENSO reaches its maximum intensity. The basin mode peaks 8 months after the IOZM. The timing and associated SST patterns suggests that the IOZM is related to ENSO, and the basin-wide warming/cooling develops as a result of the decay of the IOZM spreading SST anomalies from western Indian Ocean to the eastern Indian Ocean. In contrast, in the Indian-Ocean Run, no oscillatory modes can be identified by the MSSA, even though the Indian Ocean SST variability is characterized by east–west SST contrast patterns similar to the IOZM. In both control and anomaly runs, IOZM-like SST variability appears to be associated with forcings from fluctuations of the Indian monsoon. Our modeling results suggest that the oscillatory feature of the IOZM is primarily forced by ENSO.

1. Introduction

The recent interests in the observed east–west contrast pattern in Indian Ocean sea-surface temperature (SST) anomalies have prompted the suggestion that the Indian Ocean has its own unstable coupled atmosphere-ocean mode like El Niño-Southern Oscillation (ENSO) (e.g., Saji et al, 1999; Webster et al, 1999). This interannual SST variability is often referred to as Indian Ocean Zonal Mode (IOZM) or Indian Ocean Dipole. The IOZM is characterized by opposite polarities of SST anomalies between the western and eastern parts of the equatorial Indian Ocean, and is accompanied with zonal wind anomalies in the central Indian Ocean. The strong wind-SST coupling associated with the IOZM has been used to argue for the similarity of the phenomenon to the delayed oscillator of ENSO (Webster et al, 1999). The fact that the temporal correlation between the observed IOZM and ENSO events is not strong and that several significant IOZM events have occurred in the absence of large ENSO events have lead to the suggestion that the IOZM is independent of ENSO (Saji et al, 1999). On the other hand, there are suggestions that the IOZM is not an

independent phenomenon but forced by ENSO through changes in surface heat flux or Indian ocean circulation (e.g., Klein et al, 1999; Chambers et al, 1999; Murtugudde and Busalacchi, 1999; Venzke et al, 2000; Schiller et al, 2000; Huang and Kinter, 2002; Xie et al, 2002). There are also suggestions that the IOZM is a weak natural coupled mode of the Indian Ocean that can be amplified by ENSO during a particular season (e.g., Gualdi et al, 2003; Annamalai et al, 2003). The IOZM is also suggested as a natural part of the Asian summer monsoon and the tropospheric biennial oscillation (TBO) (e.g., Meehl and Arblaster, 2002; Loschnigg et al, 2003). The IOZM is argued to arise from the ocean-atmosphere interactions within the Indian Ocean region with links to the Pacific involved with the TBO.

A number of coupled atmosphere-ocean modeling studies have been carried out to examine the relationship between the IOZM and ENSO. Iizuka et al (2000) was among the first to simulate the IOZM using a coupled atmosphere-ocean general circulation model (CGCM). The IOZM-ENSO relation was examined via statistical analyses. Based on the weak temporal correlation between the IOZM and ENSO events in their CGCM simulation, Iizuka et al (2000) concluded that IOZM is independent of ENSO. In another CGCM study, Lau and Nath (2004) used composite and heat budget analyses to study IOZM events in a long-term simulation. They suggested that the remote influence of ENSO is the primary forcing to IOZM, although other factors (such as the annular mode in the Southern Hemisphere and the local SST forcings in the Indian Ocean and western Pacific) can also be important. The CGCM study of Gualdi et al (2003) suggested that the ENSO forces sea level pressure anomalies in the southeastern part of the Indian Ocean and initializes IOZM developments through local and remote oceanic processes. In these CGCM studies, Pacific influences are not isolated because the CGCM includes both the Indian and Pacific Oceans. Baquero-Bernal et al (2002) studied the IOZM-ENSO relation by including and excluding ENSO influences in their CGCM simulations. Their CGCM also includes both the Indian and Pacific Oceans. ENSO's influence is excluded in their no-ENSO CGCM simulation by replacing SSTs simulated by the ocean model component of the CGCM in the tropical Pacific by climatology before passing them to the atmospheric model. Together with observational analyses, Baquero-Bernal et al (2002) find no evidence for an ENSO-independent oscillatory dipole mode in the Indian Ocean SSTs.

There are modeling studies that configure coupled models to isolate the contribution of individual ocean basins to climate phenomena thought to involve both the Indian and Pacific Oceans (e.g., Chung and Nigam, 1999; Kim and Lau, 2001). For example, Kim and Lau (2001) performed model experiments with and without an interactive Indian Ocean to demonstrate the contribution of the combination of ocean basin phenomena in the TBO. We use a similar modeling approach in the present study to isolate ENSO's influence on Indian Ocean SST variability in two CGCM simulations (with and without an interactive Pacific Ocean). In the control simulation, the CGCM includes both the Indian and Pacific Oceans in its ocean model domain (the Indo-Pacific Run). This run has been shown to produce a reasonable ENSO simulation (Yu et al, 2002). Therefore, a significant ENSO influence is included in this simulation. In the second simulation, the ENSO influence is excluded in the CGCM by including only the Indian Ocean in its ocean model component and by prescribing monthly-varying climatological SSTs in the Pacific Ocean (the Indian-Ocean Run). By contrasting SST variability of the tropical Indian Ocean in these two simulations and their associated ocean-atmosphere coupling, we examine whether the IOZM is an intrinsic variability of the Indian Ocean or a forced variability influenced by ENSO. In Baquero-Bernal et al (2002), their no-ENSO experiment still allows the Indian Ocean to interact with the Pacific Ocean through the Indonesian throughflow. In the present study, the throughflow is completely blocked in our Indian-Ocean Run.

2. Model and simulation

The CGCM used in this study consists of the UCLA global atmospheric GCM (AGCM) (Suarez et al, 1983; Mechoso et al, 2000, and references therein) and the oceanic GCM (OGCM) known as GFDL Modular Ocean

Model (MOM) (Bryan, 1969; Cox, 1984; Pacanowski et al, 1991). The AGCM includes the schemes of Deardorff (1972) for the calculation of surface wind stress and surface fluxes of sensible and latent heat, Katayama (1972) for short-wave radiation, Harshvardhan et al (1987) for long-wave radiation, Arakawa and Schubert (1974) for parameterization of cumulus convection, and Kim and Arakawa (1995) for parameterization of gravity wave drag. The model has 15 layers in the vertical (with the top at 1 mb) and a horizontal resolution of 5°-longitude by 4°-latitude. The MOM includes the scheme of Mellor and Yamada (1982) for parameterization of subgrid-scale vertical mixing by turbulence processes. The surface wind stress and heat flux are calculated hourly by the AGCM, and the daily averages passed to the OGCM. The SST is calculated hourly by the OGCM, and its value at the time of coupling is passed to the AGCM. The model has 27 layers in the vertical with 10 m resolution in the upper 100 m. The longitudinal resolution is 1°, the latitudinal resolution varies gradually from $1/3°$ between 10° S and 10° N to almost 3° at 50° N. Figure 1 shows the domains covered by MOM in the Indo-Pacific and Indian-Ocean Runs. Outside the oceanic model domain, SSTs for the AGCM are prescribed with a monthly-varying SST climatology. SSTs poleward of 20° S and 30° N are relaxed toward their climatological values. Zonal and meridional currents are set to zero along the lateral boundary.

The Indo-Pacific and Indian-Ocean Runs are integrated for 59 and 58 years, respectively. Only the last 40 years of the simulations are analyzed in this study. The long-term mean SSTs simulated by these two CGCM experiments are compared in Fig. 1 with a 40-year (1961–2000) mean SST field from the GISST data (Rayner et al, 1996). The figure shows that both CGCM runs produce reasonably realistic simulations of the mean SSTs in the Pacific and Indian Oceans, with a warm pool (SST greater than 28 °C) that covers both the tropical western Pacific Ocean and the eastern Indian Ocean. The CGCM has a warm bias in the tropical eastern Pacific due to undersimulated amounts of stratocumulus clouds (Yu and Mechoso, 2001). The model's performance in simulating the seasonal variations of SST and monsoon circulation in the Indian Ocean is examined in Fig. 2. It shows

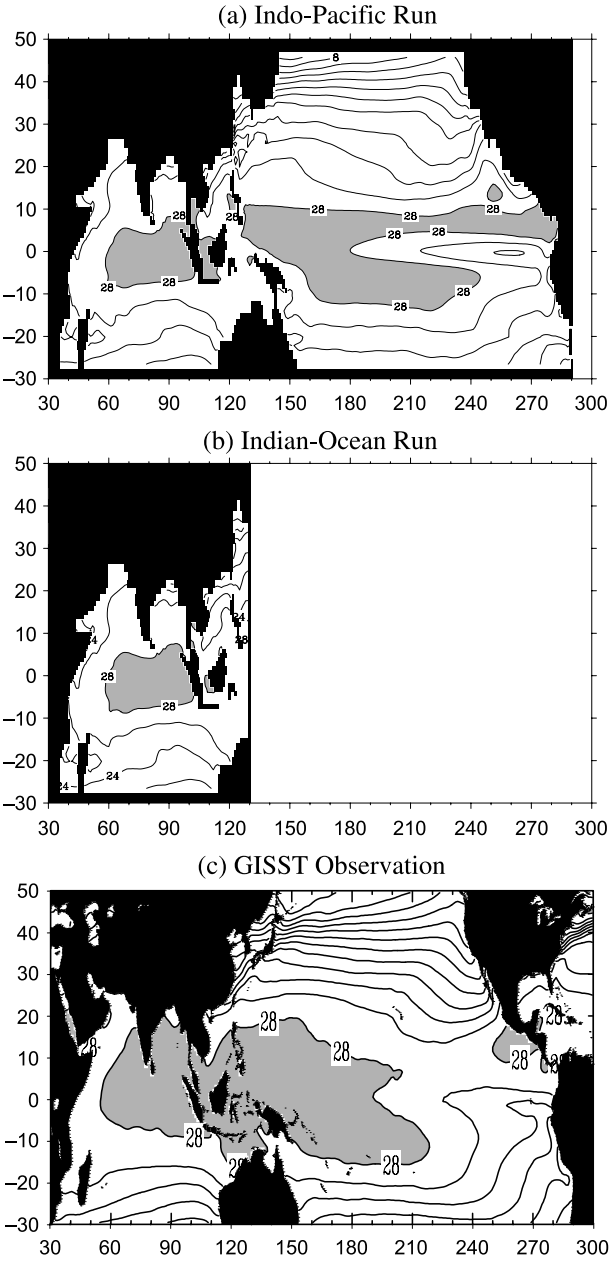

Fig. 1. Mean SSTs simulated by (**a**) the Indo-Pacific Run, (**b**) the Indian-Ocean Run, and (**c**) from GISST observation. Also shown in (**a**) and (**b**) are the sea/land masks used in these two CGCM runs. Contour intervals are 2 °C. Values greater than 28 °C are shaded

the mean spring (March–April–May), summer (June–July–August), autumn (September–October–November), and winter (December–January–February) SSTs and surface wind stresses produced by the Indo-Pacific Run. The seasonal migration of the Indian Ocean SST is reasonably simulated. The local maximum of model SSTs moves from the northern Indian Ocean in the summer to south of the equator in

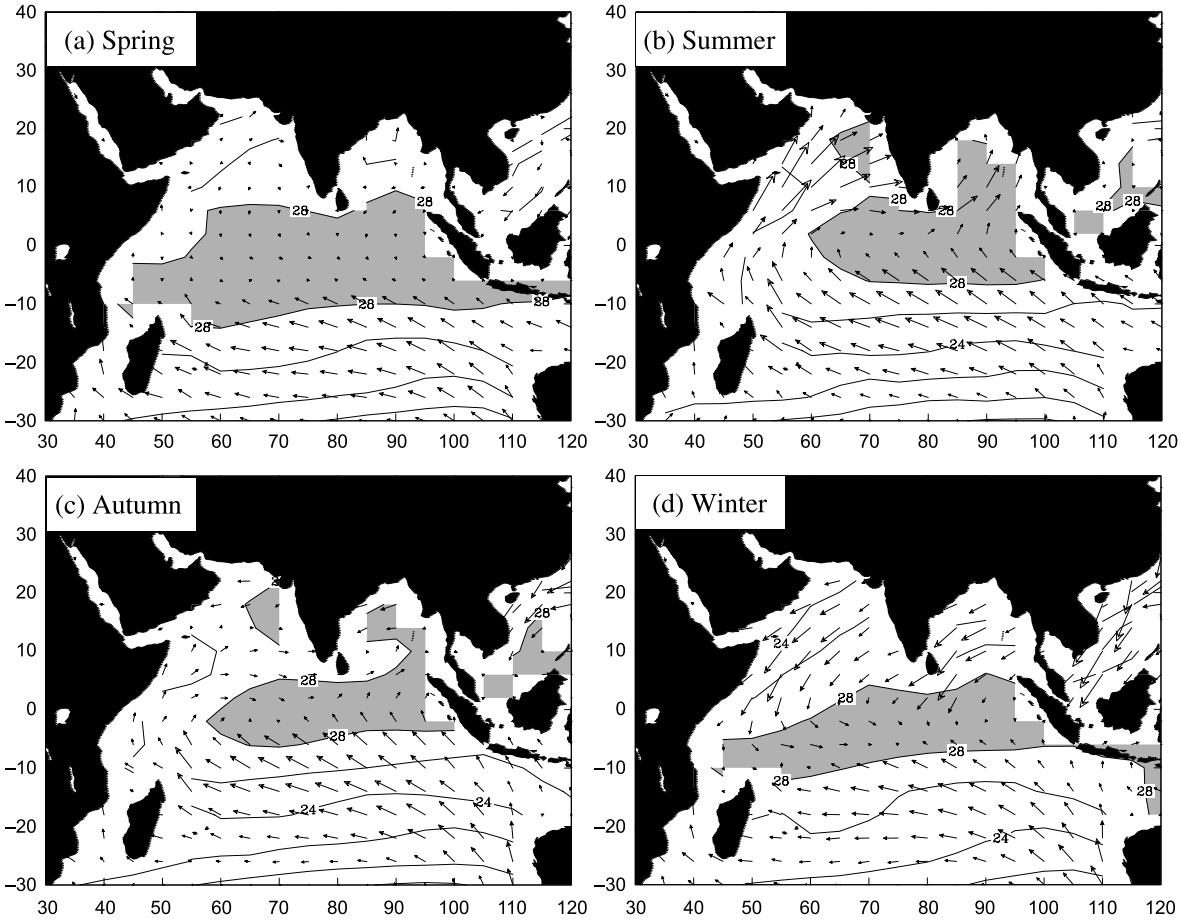

Fig. 2. Seasonal-mean SST (contours) and surface wind stress (vectors) simulated by the Indo-Pacific Run in (**a**) spring (March–April–May), (**b**) summer (June–July–August), (**c**) autumn (September–October–November), and (**d**) winter (December–January–February). Contour intervals are 2 °C for SST. SSTs greater than 28 °C are shaded. All values are shown on AGCM grids

the winter. In spring and autumn, the warm SSTs are centered at the equatorial Pacific between 10° S and 10° N. The seasonal reversals of surface winds associated with the Indian monsoon are also well simulated by the CGCM, with strong northward winds in the summer and strong southward winds in the winter near the Somali coast. The seasonal variations produced in the Indian-Ocean Run are similar to the Indo-Pacific Run and are not shown here.

3. Interannual variability in the Indo-Pacific Run

Figure 3 compares the standard deviations of the interannual SST variability in the Indo-Pacific Run and the GISST data set. The interannual SST anomalies are obtained by removing the long-term mean annual cycle and by filtering out variations with timescales shorter than one year. SSTs on OGCM grids are used here to calculate the standard deviations. In the rest of the analyses, SSTs on AGCM grids are used to facilitate analyses of atmosphere-ocean coupling. In the observations, there are four major regions of large interannual SST variability in the Indian Ocean: southwestern Indian Ocean, Bay of Bengal, off Java and Sumatra, and off Somalia. The Indo-Pacific Run produces reasonably large SST variability in these four regions of the Indian Ocean, although the model produces an unrealistic variability maximum along 5° N.

We use multi-channel singular spectrum analysis (MSSA) (Keppenne and Ghil, 1992) to identify the dominant modes of variability in the Indian Ocean from the Indo-Pacific Run. MSSA is an extension of the principal component analysis of a time series of spatial vectors

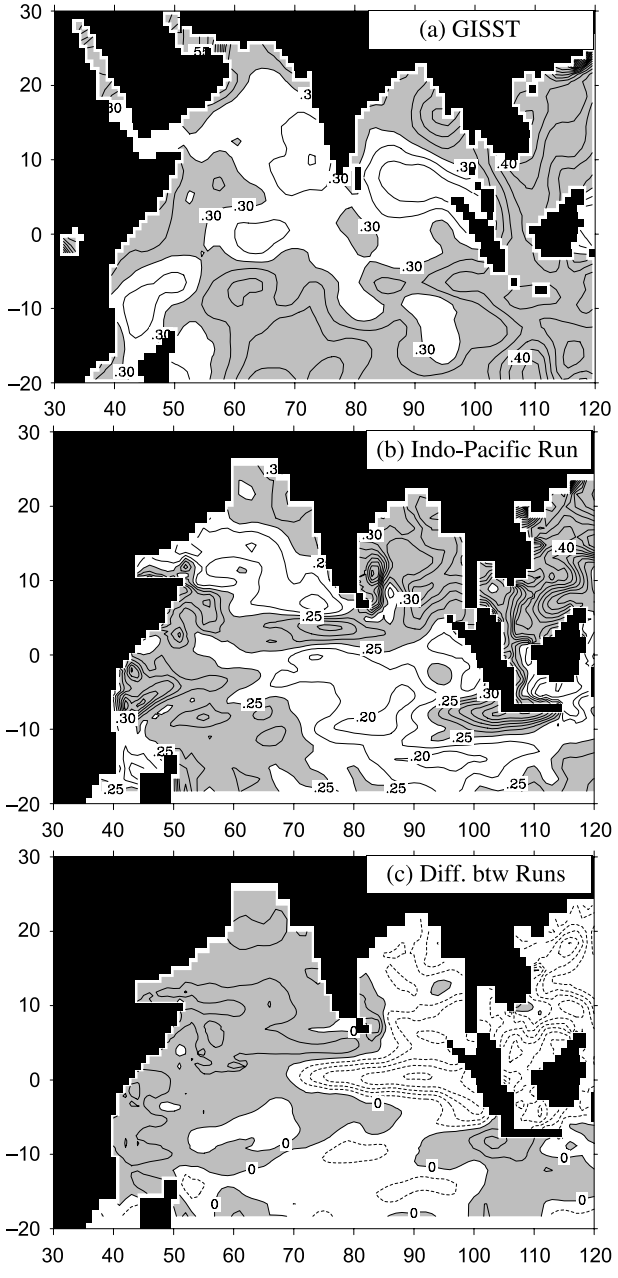

Fig. 3. Standard deviation (STD) of the interannual SST anomalies from (**a**) the GISST observations (1961–2000) and (**b**) the Indo-Pacific Run. The STD difference between the Indo-Pacific Run and the Indian-Ocean Run (the former minus the latter) is shown in (**c**). Contour intervals are 0.25 °C in (**a**) and (**b**) and are 0.04 °C in (**c**). The shading indicates values greater than 0.30 °C in (**a**), 0.25 °C in (**b**), and 0 °C in (**c**)

to include additionally an analysis of temporal structure. One major advantage of MSSA is that it easily identifies oscillatory behavior, even if it is not purely sinusoidal (Robertson et al, 1995). In MSSA, an oscillatory mode appears as a pair of MSSA modes that have similar eigenvalues,

Table 1a. Eigenvalues (in % of explained variance) of the first 10 MSSA modes of the Indo-Pacific Run

Mode	1	2	3	4	5	6	7	8	9	10
Eigenvalue (%)	8.6	7.9	5.1	5.0	4.1	3.8	3.2	3.1	3.0	2.9

similar sinusoidal principal components in quadrature with each other, and similar eigenvector structures. The MSSA can reveal correlations between atmospheric and oceanic anomalies if it is applied to combined atmospheric and oceanic variables. We apply the MSSA to model fields of SST and surface wind stress anomalies in the tropical Indian Ocean between 40° E–110° E and 30° S–30° N. A window length of 61 monthly lags is used in the MSSA.

Table 1a shows the eigenvalues for the leading 10 MSSA modes obtained from the Indo-Pacific Run. It shows that the first two MSSA modes are well separated from the rest of the spectra and have close eigenvalues. These two modes together explain about 17% of the combined variance. Their principal components are close to sinusoidal and are in quadrature with each other (not shown). Further examination reveals that these two modes also have similar eigenvector structures. Therefore, the first two MSSA modes

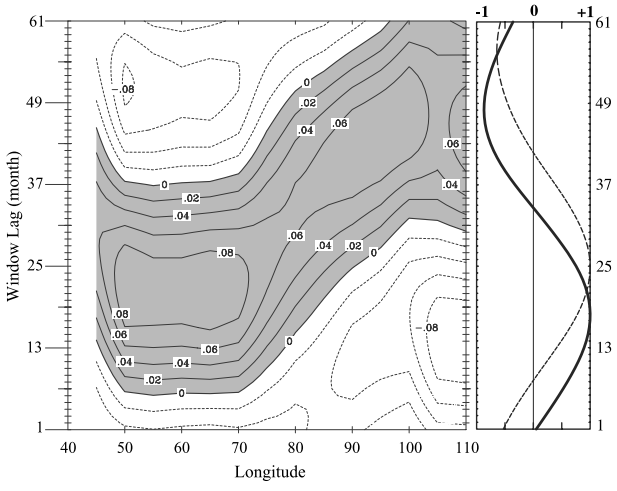

Fig. 4. The left panel shows the eigenvector structure of SST anomalies along the equator from the first MSSA mode of the Indo-Pacific Run. Contour intervals are 0.02 °C. Positive values are shaded. The right panel shows the variations of the IOZM index (thick-solid line) and the basin-wide index (thin-dashed line) calculated from the eigenvector. (See text for the definitions of both indices). The indices are scaled by their corresponding maximum values. Therefore, the index values range from −1 to +1

together represent an oscillatory cycle in the Indian Ocean. Figure 4 exhibits the longitude-time variation of the first MSSA mode at the equatorial Indian Ocean (averaged between 4° S and 4° N). The structure of the second MSSA mode is similar to this, except with a phase shift. This figure shows that the evolution of SST anomalies in the oscillatory mode at its peak is characterized by an east–west SST anomaly contrast at the equator similar to that of the IOZM.

A power spectral analysis of the principal component of this MSSA mode reveals that the leading MSSA oscillatory mode has a dominant timescale of about 4.4 years (not shown). This periodicity is close to that of the simulated ENSO cycle in the same run (shown in Yu et al, 2002). To link the first MSSA mode to the inter-annual SST variability in the Pacific Ocean, we calculate the time-lag correlation coefficients between the principal component of the first MSSA mode and SST anomalies in the entire Indo-Pacific Ocean. Figure 5 shows that the correlation is characterized by an IOZM pattern in the Indian Ocean and an ENSO pattern in the Pacific. The ENSO pattern peaks about 3–5 months before the IOZM peaks. We also apply the MSSA analysis to combined SST-wind stress anomalies produced by the Indo-Pacific Run in the entire Indo-Pacific Ocean (40° E–80° W; 30° S–30° N). The leading two MSSA modes have similar eigen values, eigen vectors, and principal components, and together represent an oscillatory mode in the Indo-Pacific Ocean. The eigenvector structure of SST anomalies along the equator from this oscillatory mode (not shown) is similar to the patterns shown in Fig. 5.

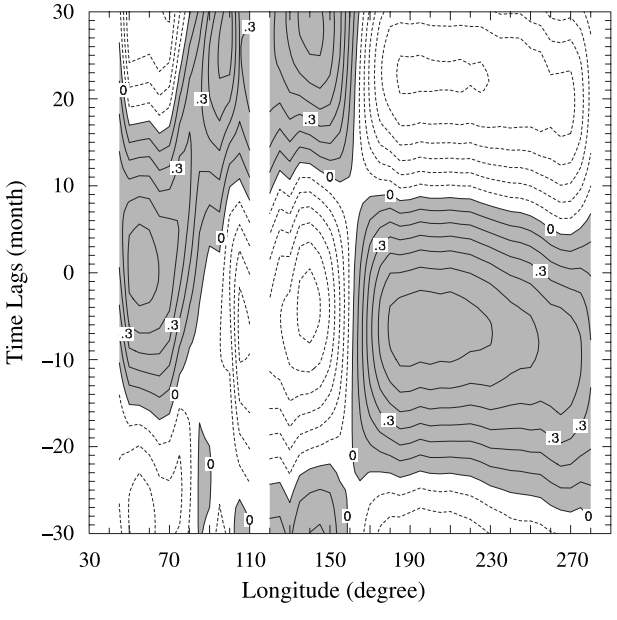

Fig. 5. Time-lag correlation coefficients between the principal component of the first MSSA mode of Fig. 4 and the low-pass filtered SST anomalies in the Indo-Pacific Run. Values are averaged between 4° S and 4° N. Contour intervals are 0.1. Positive values are shaded

The close connection between IOZM and ENSO in the MSSA and correlation analyses, together with the similar oscillatory periodicity, suggest that the IOZM-like oscillatory mode shown in Fig. 4 is related to ENSO. We also examine the time series of the NINO3 index (SST anomalies in 90°–150° W; 5° S–5° N) and the IOZM index from the Indo-Pacific Run. Following Saji et al (1999), the IOZM index is defined as the SST anomaly difference between the western Indian Ocean (50° E∼70° E and 10° S∼10° N) and the eastern Indian Ocean (90° E∼110° E and 10° S∼0°). It is found that the major IOZM and ENSO events coincide with each other during the simulation (not shown), although the simultaneous correlation coefficient between them is only 0.5.

It is noted in Fig. 4 that a basin-wide warming/cooling pattern also appears during the evolution of the first MSSA mode. The basin-wide SST pattern emerges when the east–west SST contrast pattern decays and spreads SST anomalies from the western Indian Ocean to the eastern Indian Ocean. This slow eastward propagation of warm SST anomalies during the decay phase of the IOZM is consistent with that observed by Feng and Meyers (2003). We use an IOZM index and a basin-wide index in Fig. 4 to examine the time lags between the east–west contrast pattern and the basin-wide pattern in the leading MSSA mode. Following An (2004), the basin index is defined as the domain average SST anomalies over the tropical Indian Ocean (45° E∼105° E, 15° S∼10° N). The index values shown in Fig. 4 indicate that the peak of the IOZM mode occurs at month 18 of the M-SSA mode and is followed by the peak of the basin-wide mode about 8 months later. After the demise of the basin-wide warming, a negative phase of the IOZM merges.

The evolution from the east–west contrast pattern to the basin-wide pattern can be better seen in Fig. 6, which shows the Indian Ocean SST

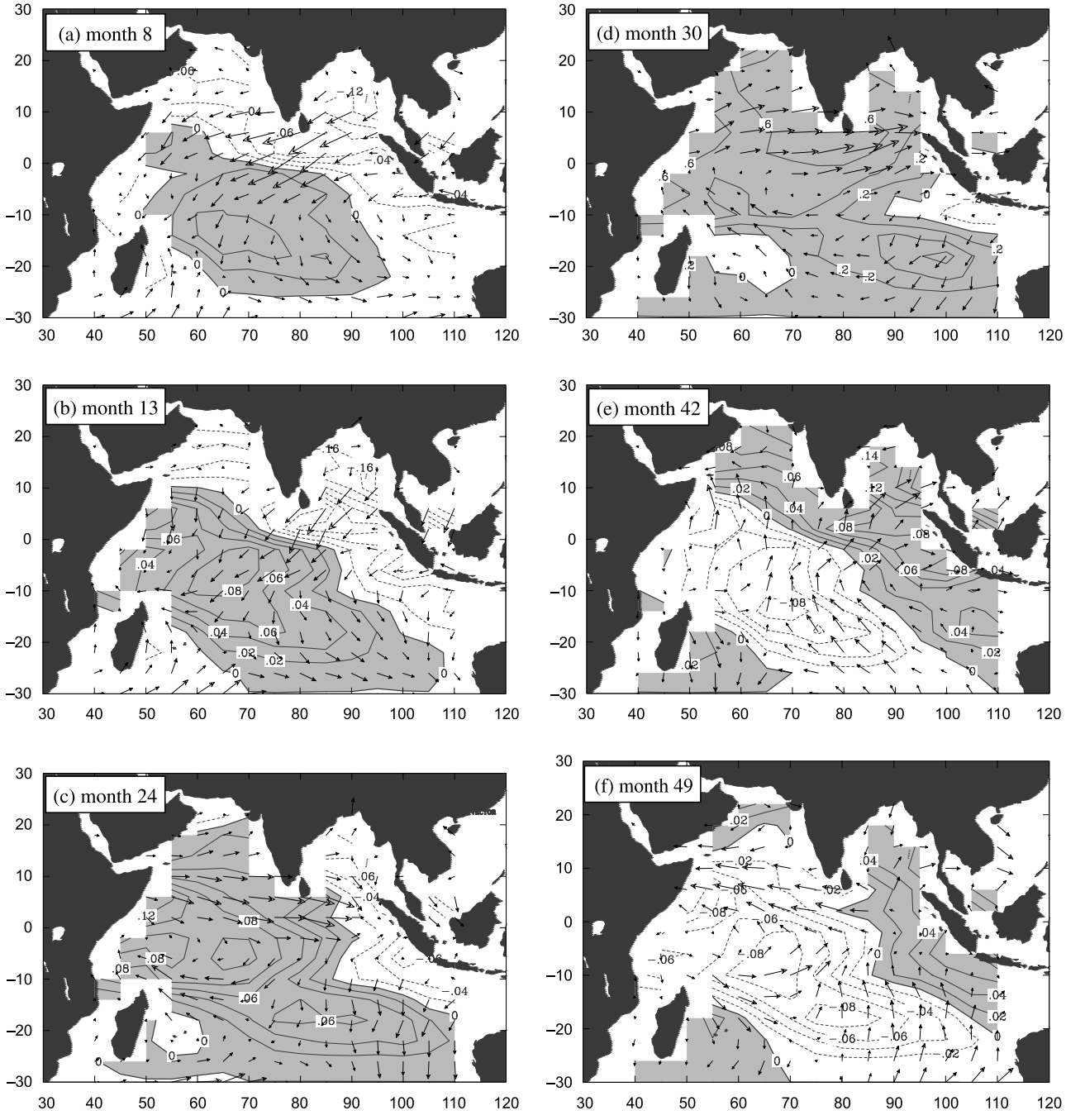

Fig. 6. Evolutions of SST and wind stress anomalies of the first MSSA mode from the Indo-Pacific Run. The month shown in the upper left corner of each panel corresponds to the window lag of Fig. 4. SST anomalies are shown by contours with an interval of 0.02 °C. Wind stress anomalies are shown by vectors

anomalies during various stages of the leading MSSA mode. Figure 6a and b shows the onset and growing stages of the positive phase of the oscillatory mode, which are characterized by intensifying positive and negative SST anomalies in the western and eastern Indian Ocean respectively. After the east–west SST contrast reaches its peak amplitude (at about month 18 of Fig. 4), a basin-wide warming emerges as a result of the warm SST anomalies spreading from the western Indian Ocean to the eastern Indian Ocean (Fig. 6c and d). The basin-wide warming is followed by a negative phase of the oscillatory mode (Fig. 6e). After the decay of the negative phase, a basin-wide cooling pattern emerges (Fig. 6f).

This MSSA analysis suggests that both the basin-wide pattern (also referred as the monopole mode in some studies) and the IOZM are related and are part of the cycle of an ENSO-related oscillatory mode in the Indian Ocean. This is consistent with observational finding that these two patterns of Indian Ocean SST variability are significant correlated at leads and lags of around 9–10 months (Allan et al, 2001). Based on Figs. 4 and 5, the time sequence of this oscillation mode in the Indo-Pacific Run is as such: a positive (negative) phase of the IOZM peaks about 3–5 months after the warm (cold) ENSO reaches its maximum intensity and is followed by a basin-wide warming (cooling) pattern about 8 months later. A recent observational study of An (2003) also suggests that the IOZM and the basin-wide mode are related. However, his EOF study suggests that the IOZM is resulted from the basin-wide mode. In his analysis, about 3–6 months after a warm ENSO event, a basin-wide warming mode of SST anomalies appears in the Indian Ocean. After the demise of the basin-wide warming, a negative phase of the IOZM mode develops. This sequence described by An (2003) is similar to the SST evolutions during months 31–61 of our leading MSSA mode shown in Figs. 4 and 5.

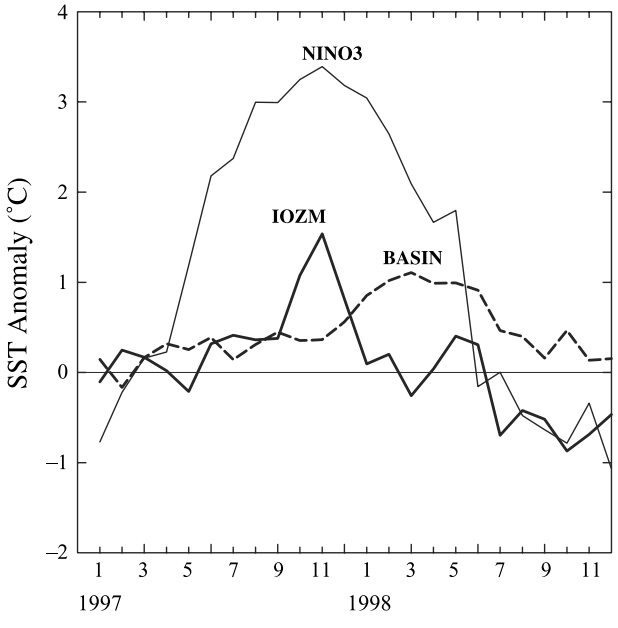

Fig. 7. Variations of NINO3 (think-solid), IOZM (thick-solid), and basin-wide (thick-dashed) indices for the 1997–1998 El Niño event. The SST anomalies are calculated from the GISST data set with the long-term (1961–2000) seasonal cycle removed

The time sequence simulated in our Indo-Pacific Run appears close to the sequence observed during the 1997–98 ENSO event (e.g., Yu and Rienecker, 1999; 2000; Murtugudde et al, 2000), although discrepancies exit. Figure 7 shows the values of the NINO3, IOZM, and basin-wide indices calculated from the GISST SST for the 1997–98 ENSO event. The NINO3 index shows that the 1997–98 ENSO grew during summer of 1997 and reached its peak near November 1997. During this ENSO event, an IOZM feature also peaked in November of 1997. A basin-wide warming showed up later and peaked in March and May of 1998. One discrepancy between this observed time sequence and our model sequence is that, in the Indo-Pacific Run, ENSO peaks earlier than does the IOZM. We find that this discrepancy may be due to the fact that the model ENSO tends to peak in early fall, rather than in winter as observed. It is evident in Fig. 8a, where the normalized standard deviation (STD) anomalies of the NINO3 index calculated from the Indo-Pacific Run are shown as a function of the calendar month. The normalized anomalies are obtained by removing the annual mean value of STD and by normalizing the anomalies with the standard deviation of the STD anomalies. This figure shows that the model ENSO has the largest intensity in September. Also shown in Fig. 8 are the normalized STD anomalies of the IOZM index and the basin-wide index. Figure 8b shows that the Indo-Pacific Run realistically simulates peak IOZM variability at the end of the fall season near November. The simulated basin-wide SST variability has a peak in April, close the peak months of the basin-wide warming pattern observed in the 1997–98 ENSO event. The phase relationships observed in the 1997–98 ENSO is consistent with our suggestion that the ENSO-related IOZM pattern leads to the basin-wide warming/cooling pattern in the Indian Ocean.

The surface wind stress anomalies associated with the leading MSSA mode are also shown in Fig. 6 to examine the ocean–atmosphere coupling of the oscillatory mode. During the positive phase of this mode, the east–west SST anomaly contrast in the tropical Indian Ocean is accompanied with strong zonal wind stress anomalies along the equator (Fig. 6a and b). In addition, strong

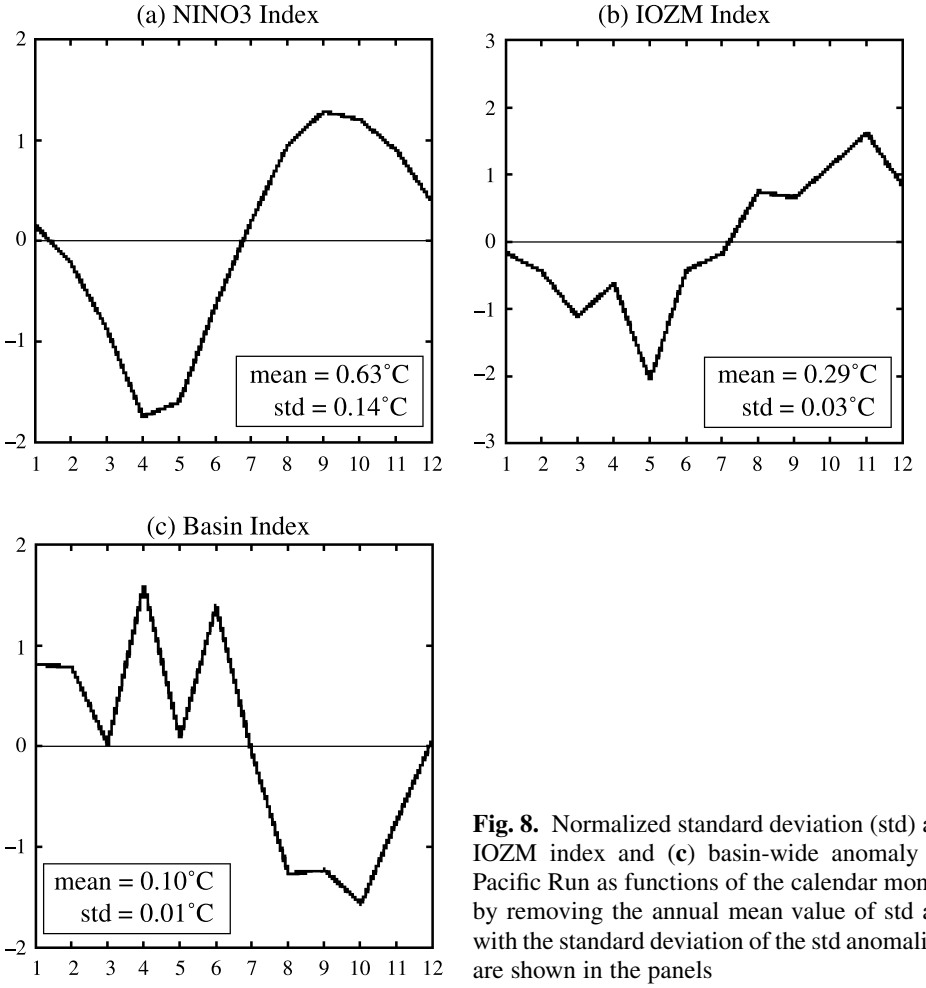

Fig. 8. Normalized standard deviation (std) anomalies of (**a**) NINO3 index, (**b**) IOZM index and (**c**) basin-wide anomaly index calculated from the Indo-Pacific Run as functions of the calendar month. The values shown are obtained by removing the annual mean value of std and by normalizing the anomalies with the standard deviation of the std anomalies. The mean and std of each index are shown in the panels

cross-hemisphere circulation anomalies are present. Surface wind anomalies cross the equator from the northern hemisphere into the southern hemisphere along the east coast of the Africa. This feature represents a relaxation of the Indian summer monsoon circulation. This anomalous circulation pattern can weaken the upwelling associated with the low-level Somali Jet near the African coast and lead to the warming of the ocean surface in this region. Over the eastern Indian Ocean, stronger off-shore surface wind anomalies are produced near Sumatra. These wind patterns can enhance coastal upwelling near Sumatra and lead to the cooling of the ocean surface in this region. During the decaying stage of the east–west SST contrast pattern (Fig. 6c), the warm SST anomalies begin to spread eastward from the western Indian Ocean to the eastern Indian Ocean. Surface wind stresses along the equator are weakened and westerly anomalies begin to increase. A few months later, a basin-wide warming pattern is present in the tropical Indian Ocean (Fig. 6d). After the warming, a negative phase of IOZM-like feature develops. During the negative phase of this mode, a surface wind anomaly pattern opposite that of the positive phase is produced (Fig. 6e). This pattern represents a strengthened summer monsoon circulation. Through similar upwelling mechanisms, this circulation pattern leads to cooling and warming of the ocean surface in the western and eastern Indian Ocean, respectively, in the negative phase. The SST-wind stress relations shown in this mode are close to those found for observed IOZM events (Saji et al, 1999; Webster et al, 1999).

4. Interannual variability in the Indian-Ocean Run

We now turn to the interannual SST variability produced in the Indian-Ocean Run. Table 1b lists the eigenvalues of the leading 10 MSSA modes

Table 1b. Eigenvalues (in % of explained variance) of the first 10 MSSA modes of the Indian-Ocean Run

Mode	1	2	3	4	5	6	7	8	9	10
Eigenvalue (%)	8.1	7.2	6.0	5.2	4.8	4.5	4.0	3.9	3.2	3.1

obtained from this CGCM run. It shows no pair of MSSA modes with similar eigenvalues. In addition, the eigenvalues of leading MSSA modes are not well separated from the other modes. Further examination reveals no pair of MSSA modes with similar principal components, and eigenvector structures (not shown). This indicates that no oscillatory mode of variability can be identified by MSSA in the Indian Ocean for the Indian-Ocean Run. It is noticed that the first six MSSA modes all have as a major feature on east–west SST anomaly contrast along the equator, similar to that of the IOZM. They together explain 35% of the combined variance. We only show the eigenvector structures of SST anomalies for the first four MSSA modes in Fig. 9 to show their similarity. These figures indicate that the dominant timescale of these equatorial SST anomaly contrast patterns varies from about 10 years in the first mode to about 2–3 years in the fourth mode. The timescale decreases to about 1.5 year for the sixth MSSA mode (not shown). One implication from these leading MSSA modes is that IOZM-like features can be associated with intrinsic variability of the Indian Ocean over a wide range of timescales. However, this east–west SST variability does not have the characteristics of a self-sustained oscillation. The abundance of these IOZM-like features with no preferred timescales in the Indian Ocean suggests that IOZM should not be considered as fully coupled oscillator like ENSO. Rather, it should be considered as a generic feature of the Indian Ocean that can often be produced by large scale remote forcing such as ENSO, as well as by atmospheric monsoon forcings.

We have also examined the ocean–atmosphere coupling associated with the leading six MSSA modes of the Indian-Ocean Run and found that they all exhibit a major association with monsoon-type circulation changes. Figure 10a and b displays the positive and negative phases of the fourth MSSA mode, respectively. We choose to display this mode because it goes through one

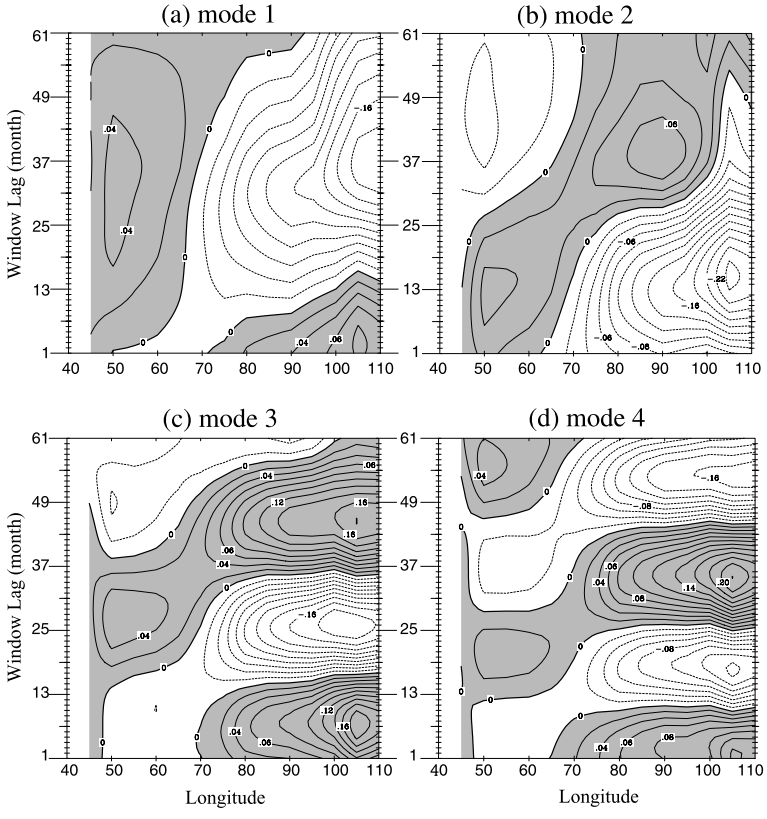

Fig. 9. Eigenvector structure of SST anomalies along the equator from the first four MSSA modes of the Indian-Ocean Run. Contour intervals are 0.02 °C. Positive values are shaded

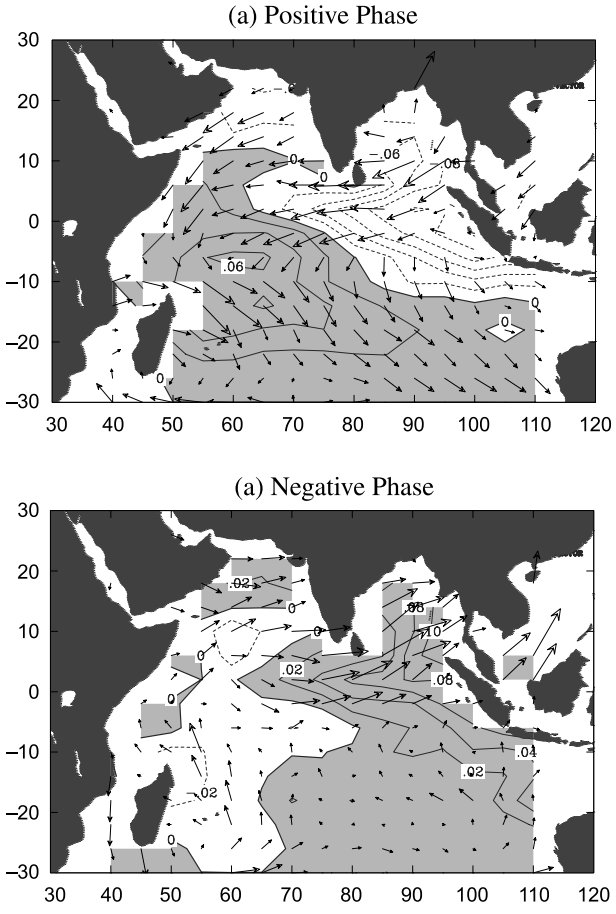

Fig. 10. Same as Fig. 6, except for the fourth MSSA mode from the Indian-Ocean Run during the mature stages of its (**a**) positive phase and (**b**) negative phase

complete cycle during the 61-month window used in the MSSA analysis (see Fig. 9d). The positive and negative phases of this mode are also associated with a relaxed and enhanced Indian monsoon circulation pattern, respectively, similar to those of the IOZM mode in the Indo-Pacific Run. This similarity suggests that IOZM-like variability in both the Indo-Pacific and Indian-Ocean Runs are related to variations in the Indian monsoon circulation.

5. Conclusions and discussions

By comparing Indian Ocean SST variability produced by two CGCM simulations including and excluding the Pacific Ocean, the intrinsic and forced SST variability in the Indian Ocean has been examined. The comparisons indicate that an oscillatory mode with IOZM-like features, followed by a basin-wide warming/cooling pattern, can be identified in the Indian Ocean when the ENSO influence is included in the coupled model. This oscillatory mode has a dominant timescale similar to ENSO. The IOZM peaks about 3–5 months after ENSO reaches its maximum intensity. The basin-wide warming/cooling in the Indian Ocean emerges about 8 months after the IOZM peaks. The timing and the accompanying wind and SST variation suggest that the IOZM is directly forced by ENSO, and the basin-wide warming/cooling stems from the decay of the IOZM spreading SST anomalies from the western Indian Ocean to the eastern Indian Ocean. No oscillatory mode can be found with the MSSA method in the Indian Ocean when the ENSO influence is excluded in the Indian-Ocean Run. However, east–west SST anomaly contrast features similar to IOZM can be easily found in the leading MSSA modes of the Indian Ocean. Examination of these IOZM-like features in the Indian-Ocean Run reveals a similar association with enhanced and weakened monsoon-type circulations, as in the Indo-Pacific run. This association suggests that IOZM-like variability is forced by changes in wind and surface heat fluxes associated with fluctuations of the Indian monsoon (Yu and Rienecker, 1999). Our results indicate that IOZM-like features can occur even in the absence of large ENSO events in the Pacific. However, the oscillatory feature of the IOZM is forced by ENSO.

It is interesting to note that the IOZM-like fluctuations in the Indian-Ocean Run have larger SST anomalies in the eastern Indian Ocean and that the IOZM-like mode in the Indo-Pacific Run has larger SST anomalies in the western Indian Ocean (compare Fig. 9a–d to Fig. 4). This difference is also reflected in the standard deviation of SST anomalies produced in these two runs. Figure 3c displays the differences between standard deviations of interannual SST anomalies produced in the Indo-Pacific Run and those in the Indian-Ocean Run. It shows that most of the large differences appear in the tropical Indian Ocean. With ENSO's influence, the SST variability produced in the Indo-Pacific Run is smaller (than the Indian-Ocean Run) in the eastern Indian Ocean and larger in the western Indian Ocean. The central locations of the reduced and increased variability are close to the eastern and western centers of the IOZM. This coincidence suggests that the relative

strength of the IOZM-like variability is also influenced by ENSO.

In summary, the present modeling study suggests that IOZM-like variability in the Indian Ocean is a forced response to Indian monsoon variability. ENSO acts as a strong pace maker to the IOZM that can affect both the dominant timescale and east–west structures of the IOZM. It should be noted that the CGCM used in this study tends to produce more regular ENSO cycles than the observed. It is yet to be determined whether or not this too-regular ENSO recurrence affects ENSO's influence on the Indian Ocean SST variability. The conclusions reported in this study can be model dependent.

Acknowledgments

The authors would like to thank three anonymous reviewers for their helpful comments on the manuscript. The research was supported by NOAA CLIVAR-Pacific Program under Grant NA03OAR4310061. Model integrations were performed at the San Diego Supercomputer Center with computer allocations provided by NPACI. KML was supported by the NASA Global Modeling and Data Analysis Program.

References

Allan R, Chambers D, Drosdowsky W, Hendon H, Latif M, Nicholls N, Smith I, Stone R, Tourre Y (2001) Is there an Indian Ocean dipole, and is it independent of the El Niño-Southern Oscillation? CLIVAR Exchanges 6: 18–22

An S-I (2004) A dynamical linkage between the monopole and dipole modes in the tropical Indian Ocean. Theor Appl Climatol 78: 195–201

Annamalai H, Murtugudde R, Potemra J, Xie SP, Liu P, Wang B (2003) Coupled dynamics over the Indian Ocean: Spring initialization of the zonal mode. Deep-Sea Research II 50: 2305–2330

Arakawa A, Schubert WH (1974) Interaction of a cumulus cloud ensemble with the large-scale environment, Part I. J Atmos Sci 31: 674–701

Baquero-Bernal A, Latif M, Legutke S (2002) On Dipole like variability of sea-surface temperature in the Tropical Indian Ocean. J Climate 15: 1358–1368

Bryan K (1969) A numerical method for the study of the circulation of the world ocean. J Comp Phys 4: 347–376

Chambers DP, Tapley BD, Stewart RH (1999) Anomalous warming in the Indian Ocean coincident with El Niño. J Geophys Res 104: 3035–3047

Chung C, Nigam S (1999) Asian summer monsoon-ENSO feedback on the Cane-Zebiak model ENSO. J Climate 12: 2787–2807

Cox MD (1984) A primitive equation three-dimensional model of the ocean. GFDL Ocean Group Tech. Rep. No. 1

Deardorff JW (1972) Parameterization of the planetary boundary layer for use in general circulation models. Mon Wea Rev 100: 93–106

Feng M, Meyers G (2003) Interannual variability in the tropical Indian Ocean: A two-year time-scale of Indian Ocean Dipole. Deep-Sea Research II 50: 2263–2284

Gualdi S, Guilyardi E, Navarra A, Masina S, Delecluse P (2003) The interannual variability in the tropical Indian Ocean. Clim Dyn 20: 567–582

Harshvardhan RD, Randall DA, Corsetti TG (1987) A fast radiation parameterization for general circulation models. J Geophys Res 92: 1009–1016

Huang B, Kinter JL (2002) The interannual variability in the tropical Indian Ocean and its relations to El Niño-Southern Oscillation. J Geophys Res 107: 3199 (DOI: 10.1029/2001J C001278)

Iizuka S, Matsuura T, Yamagata T (2000) The Indian Ocean SST dipole simulated in a coupled general circulation model. Geophys Res Lett 27: 3369–3372

Katayama A (1972) A simplified scheme for computing radiative transfer in the troposphere. Numerical Simulation of Weather and Climate Tech. Rep. No. 6, Dept. of Atmospheric Sciences, University of California, Los Angeles, CA, 77 pp

Keppenne CL, Ghil M (1992) Adaptive spectral analysis and prediction of the Southern Oscillation Index. J Geophys Res 97: 20449–20454

Kim K-M, Lau K-M (2001) Dynamics of monsoon-induced biennial variability in ENSO. Geophys Res Lett 28: 315–318

Kim Y-J, Arakawa A (1995) Improvement of orographic gravity-wave parameterization using a mesoscale gravity-wave model. J Atmos Sci 52: 1875–1902

Klein SA, Soden BJ, Lau NC (1999) Remote sea-surface temperature variations during ENSO: Evidence for a tropical atmospheric bridge. J Climate 12: 917–932

Lau N-C, Nath MJ (2004) Coupled GCM simulation of atmosphere–ocean variability associated with zonally asymmetric SST changes in the tropical Indian Ocean. J Climate 17: 245–265

Loschnigg J, Meehl GA, Webster PJ, Arblaster JM, Compo GP (2003) The Asian monsoon, the tropospheric biennial oscillation and the Indian Ocean Dipole in the NCAR CSM. J Climate 16: 2138–2158

Mechoso CR, Yu J-Y, Arakawa A (2000) A coupled GCM pilgrimage: From climate catastrophe to ENSO simulations. In: General circulation model development: Past, present, and future (Randall DA, ed). Academic Press (forthcoming)

Meehl GA, Arblaster JM (2002) The tropospheric biennial oscillation and Asian-Australian monsoon rainfall. J Climate 15: 722–744

Mellor GL, Yamada T (1982) Development of a turbulence closure model for geophysical fluid problems. Rev Geophys Space Phys 20: 851–875

Murtugudde R, Busalacchi AJ (1999) Interannual variability of the dynamics and thermodynamics of the tropical Indian Ocean. J Climate 12: 2300–2326

Murtugudde R, McCreary JP, Busalacchi AJ (2000) Oceanic processes associated with anomalous events in the Indian

Ocean with relevance to 1997–1998. J Geophys Res 105: 3295–3306

Pacanowski RC, Dixon KW, Rosati A (1991) The GFDL Modular Ocean Model user guide. Tech. Rep. 2, GFDL Ocean Group

Rayner NA, Horton EB, Parker DE, Folland CK, Hackett RB (1996) Version 2.2 of the global sea-ice and sea surface temperature data set, 1903–1994, CRTN 74, Available from Hadley Centre, Met Office, Bracknell, UK

Robertson AW, Ma C-C, Ghil M, Mechoso CR (1995) Simulation of the tropical Pacific climate with a coupled ocean-atmosphere general circulation model. Part II: Interannual variability. J Climate 8: 1199–1216

Saji NH, Goswami BN, Vinayachandran PN, Yamagata T (1999) A dipole mode in the tropical Indian Ocean. Nature 401: 360–363

Schiller A, Godfrey JS, McIntosh PC, Meyers G, Fielder R (2000) Interannual dynamics and thermodynamics of the Indo-Pacific Oceans. J Phys Oceanogr 30: 987–1012

Suarez MJ, Arakawa A, Randall DA (1983) The parameterization of the planetary boundary layer in the UCLA general circulation model: Formulation and results. Mon Wea Rev 111: 2224–2243

Venzke S, Latif M, Vilwock A (2000) The coupled GCM ECHO-2, II, Indian Ocean response. J Climate 13: 1371–1383

Webster PJ, Moore A, Loschnigg J, Leban M (1999) Coupled ocean-atmosphere dynamics in the Indian Ocean during 1997–98, 23 September. Nature 40: 356–360

Xie SP, Annamalai H, Schott FA, McCreary JP (2002) Structure and mechanisms of south Indian Ocean climate variability. J Climate 15: 867–878

Yu J-Y, Mechoso CR (2001) A coupled atmosphere–ocean GCM study of the ENSO cycle. J Climate 14: 2329–2350

Yu J-Y, Mechoso CR, McWilliams JC, Arakawa A (2002) Impacts of the Indian Ocean on the ENSO cycle. Geophys Res Lett 29: 461–464

Yu LS, Rienecker MM (1999) Mechanisms for the Indian Ocean warming during the 1997–98 El Niño. Geophys Res Lett 26: 735–738

Yu LS, Rienecker MM (2000) Indian Ocean warming of 1997–1998. J Geophys Res 105: 16923–16939

Corresponding author's address: Dr. Jin-Yi Yu, Department of Earth System Science, University of California at Irvine, Croul Hall 3315, Irvine, CA 92697-3100, USA (E-mail: jyyu@uci.edu)